



HAL
open science

Deciphering the pH-dependence of ground- and excited-state equilibria of thienoguanine

Pascal Didier, Jagannath Kuchlyan, Lara Martinez-Fernandez, Pauline Gosset, Jérémie Léonard, Yitzhak Tor, Roberto Improta, Yves Mely

► **To cite this version:**

Pascal Didier, Jagannath Kuchlyan, Lara Martinez-Fernandez, Pauline Gosset, Jérémie Léonard, et al.. Deciphering the pH-dependence of ground- and excited-state equilibria of thienoguanine. *Physical Chemistry Chemical Physics*, 2020, 22 (14), pp.7381-7391. 10.1039/C9CP06931C . hal-02941317

HAL Id: hal-02941317

<https://hal.science/hal-02941317>

Submitted on 8 Dec 2020

HAL is a multi-disciplinary open access archive for the deposit and dissemination of scientific research documents, whether they are published or not. The documents may come from teaching and research institutions in France or abroad, or from public or private research centers.

L'archive ouverte pluridisciplinaire **HAL**, est destinée au dépôt et à la diffusion de documents scientifiques de niveau recherche, publiés ou non, émanant des établissements d'enseignement et de recherche français ou étrangers, des laboratoires publics ou privés.

ARTICLE

Deciphering the pH-dependence of ground- and excited-state equilibria of thienoguanine

Received 00th January 20xx,
Accepted 00th January 20xx

Pascal Didier,^{*a} Jagannath Kuchlyan,^a Lara Martinez-Fernandez,^b Pauline Gosset,^a Jérémie Léonard,^c Yitzhak Tor,^d Roberto Improta^{*e} and Yves Mély^{*a}

DOI: 10.1039/x0xx00000x

The thienoguanine nucleobase (thG_b) is an isomorphous fluorescent analogue of guanine. In aqueous buffer at neutral pH, thG_b exists as a mixture of two ground-state H1 and H3 keto-amino tautomers with distinct absorption and emission spectra and high quantum yield. In this work, we performed the first systematic photophysical characterization of thG_b as a function of pH (2 to 12). Steady-state and time-resolved fluorescence spectroscopies, supplemented with theoretical calculations, enabled us to identify three additional thG_b forms, resulting from pH-dependent ground-state and excited-state reactions. Moreover, a thorough analysis allowed us to retrieve their individual absorption and emission spectra as well as the equilibrium constants which govern their interconversion. From these data, the complete photoluminescence pathway of thG_b in aqueous solution and its dependence as a function of pH was deduced. As the identified forms differ by their spectra and fluorescence lifetime, thG_b could be used as a probe for sensing local pH changes under acidic conditions.

Introduction

Numerous cellular mechanisms and pathways rely on dynamic interactions of nucleic acids with proteins that induce local and transient changes in their secondary and tertiary structures as well as in their properties and functions(1–6). Though X-ray diffraction, NMR spectroscopy or electron microscopy provide invaluable information on the structure of protein/nucleic acid complexes, they are less suited for monitoring the dynamics of these interactions and their associated changes, especially in dilute solutions. Due to their exquisite sensitivity, fluorescence-based techniques are highly effective for such purposes. Their implementation for nucleic acids, however, suffers from the lack of emissive nucleoside analogues able to reliably replace the natural nucleobases, while maintaining favorable photophysics. Indeed, although many structurally diverse nucleotide analogs exhibiting probe-like properties have been developed, most of them are strongly quenched upon incorporation into oligonucleotides (ODNs)

and/or do not properly substitute the natural nucleobases, inducing substantial changes in the conformation and dynamics of the labeled sequences^{7–10}. This is notably the case for 2-Aminopurine (2-AP), a very popular mimic of adenosine that is strongly quenched in duplexes and alters the dynamics of the flanking base pairs(10). To overcome these limitations, efforts have been devoted to designing new generations of fluorescent nucleoside surrogates(11,12). Among these new compounds, a particularly interesting breakthrough has been recently achieved with the introduction of thienoguanosine (thG), a truly faithful emissive and responsive G surrogate, which reliably reproduces the structural context and dynamics of the parent native nucleoside(13). In addition, this fluorescent G analogue remains strongly emissive when incorporated into ODNs, and exhibits environmental sensitivity. This fluorescent nucleoside has already been extensively used to monitor protein/ODN interactions(6,14,15), protein-induced base flipping(16), conformational changes in ODNs(6,17), single nucleotide polymorphism(14); ribozyme-mediated cleavage processes(18), cellular activity of siRNAs(19) and distance measurements in DNA(15,20).

In a recent study, we demonstrated that thG exists as two ground-state tautomers with distinct absorption and emission spectra, and high quantum yield in aqueous buffer at neutral pH(14,21). Using quantum mechanical calculations, the two tautomers identified as the H1 and H3 keto-amino tautomers (Figure 1) were predicted to coexist both in the isolated nucleoside or when included in ODNs. Moreover, these tautomers exhibit distinct environmental sensitivity and thus provide additional data channels for analyzing G residues in ODNs and their complexes with proteins.

^a Laboratoire de Bioimagerie et Pathologies, UMR 7021 CNRS Université de Strasbourg, Faculté de pharmacie 74 route du Rhin, 67401 Illkirch, France.

^b Departamento de Química, Facultad de Ciencias, Módulo13, Universidad Autónoma de Madrid, Campus de Excelencia UAM-CSIC, Cantoblanco, 28049 Madrid, Spain.

^c Université de Strasbourg, CNRS, Institut de Physique et Chimie des Matériaux de Strasbourg, UMR 7504, F-67034 Strasbourg, France

^d Department of Chemistry and Biochemistry, University of California, San Diego, La Jolla, CA, 92093-0358, USA.

^e Consiglio Nazionale delle Ricerche, Istituto Biostrutture e Bioimmagini Via Mezzocannone 16, 80134, Napoli (Italy).

*Corresponding authors: pascal.didier@unistra.fr, robimp@unina.it and yves.mely@unistra.fr

† Footnotes relating to the title and/or authors should appear here.

Electronic Supplementary Information (ESI) available: [details of any supplementary information available should be included here]. See DOI: 10.1039/x0xx00000x

In this context, our objective was to further characterize the photophysical properties of this information-rich fluorescent nucleobase, by performing a systematic study as a function of pH (2 to 12). Steady-state and time-resolved experiments allowed us to support the existence and characterize three new charged species, as well as the equilibria between these forms and the already characterized H1 and H3 tautomers in both the ground- and excited-states. In addition, (TD)-DFT calculations were used to substantiate their structure and rationalize their observed spectroscopic properties. The characterization of the pH dependent complex equilibria between the different thG forms opens a pathway for new applications, such as pH sensing.

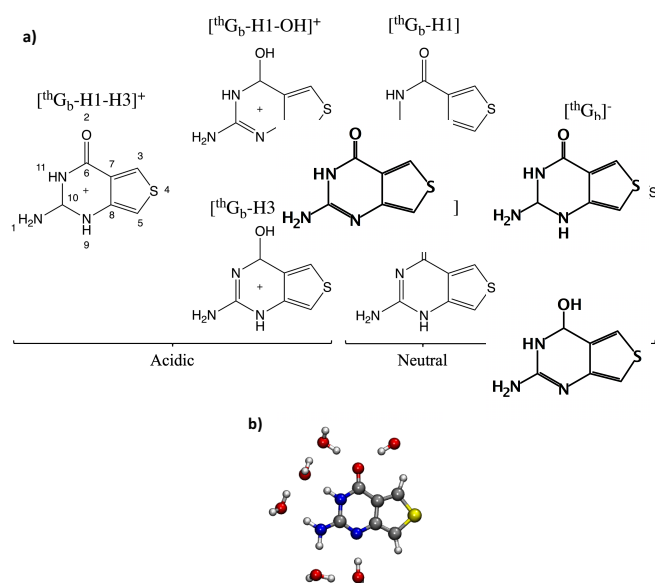


Figure 1.a) thG_b forms analyzed in the present study. The formal charge of the acidic and basic resonant forms can be located on atom 2, 9 or 11. For sake of simplicity, the charge is placed in the center of pyrimidine moiety. b) Solvation model considering 6 explicit water molecules.

Experimental section

Materials

2-amino-3H,4H-thieno[3,4-d]pyrimidin-4-one was synthesized as reported by Shin et al (2011)(13). This compound also called thienoguanine (thG_b) corresponds to the nucleobase of thG and is thus not coupled to a ribose or deoxyribose sugar. thG_b was selected for the present study, because of the large quantities of compound needed and the possible pH-dependent alterations of the sugar at extreme pHs. Stock solutions of thG_b were prepared in spectroscopic grade DMSO. For measurements at the different pH values, thG_b stock solutions were diluted at a final concentration of 12 μM in aqueous solution (<0.2% DMSO). Fresh solutions were prepared for each pH value. Solutions at pH 2 and 3 were prepared using dilute HCl. Solutions at pH 4 and 5 were prepared by using sodium 25 mM

acetate–acetic acid buffer. Solutions at pH 6 and 7 were made by using 25 mM MES and Tris buffer, respectively. For pH 8 and 9, 25mM HEPBS buffer was used. Finally, solutions at pH 10–12 were prepared using dilute NaOH. All buffer reagents were purchased from Sigma Aldrich.

Steady-State Spectroscopy

Absorption spectra were collected on a Cary 4000 UV-visible spectrophotometer (Varian). Fluorescence excitation and emission spectra were recorded at 20°C on a FluoroLog spectrofluorometer (Jobin Yvon) equipped with a thermostated cell compartment. The spectra were corrected for buffer fluorescence, lamp fluctuations, and detector spectral sensitivity. Excitation spectra of thG_b were collected at emission wavelengths of 375, 400, 450, 500, and 550 nm. For emission spectra, excitation wavelengths were at 310, 320, 330, 340, 350, 360, and 370 nm. Quantum yields (QYs) of the thG_b solutions were determined using quinine sulphate (QY=0.546 in 0.5 M H₂SO₄) as a reference(22).

Deconvolution of the absorption and emission spectra was performed based on a linear combination of the spectra of the different pure forms of thG_b. Matlab was used to determine the contributions of the different forms by using a spectral deconvolution algorithm. The ground-state pK_a values were determined by fitting the dependence of x, the relative concentrations of each species (as determined from the deconvolution of the absorption spectra) or the absorbance maxima as a function of pH with a model (1) derived from the Henderson–Hasselbalch equation, where x_{1,2} are the relative concentrations or absorption wavelengths measured at low and high pH, respectively.

$$x = \sum_{i=1,2} \frac{x_1 \times 10^{(pH-pK_{a_i})} + x_2}{1 + 10^{(pH-pK_{a_i})}} \quad (1)$$

The pK_a* values were calculated using the Förster Cycle theory with the following equation:

$$pK_a^* = pK_a - \frac{(hv_1 - hv_2)}{2.303k_B T} \quad (2)$$

where hv₁ and hv₂ are the energy of the 0–0 electronic transition of the acid and basic forms, respectively. The corresponding energies were estimated from the average of the absorption and emission maxima of the acid and basic forms(23).

Time-resolved Spectroscopy

Time-resolved fluorescence measurements were performed using time-correlated single-photon counting technique with excitation at 315 nm and 360 nm. Excitation pulses at 315 nm were generated by a pulse-picked frequency-tripled Ti-sapphire laser (Tsunami, Spectra Physics) pumped by a Millennia X laser (Spectra Physics) with a repetition rate of 4 MHz. Excitation pulses at 360 nm were generated

by a supercontinuum laser (NKT Photonics SuperK Extreme) with 10 MHz repetition rate. The fluorescence decays were collected throughout the emission spectra with 20 nm interval, using a polarizer set at magic angle and a 16 mm band-pass monochromator (Jobin Yvon). The single-photon events were detected with a micro-channel plate photomultiplier R3809U Hamamatsu, coupled to a pulse pre-amplifier HFAC (Becker-Hickl GmbH) and recorded on a time-correlated single photon counting board SPC-130 (Becker-Hickl GmbH). The instrumental response function (IRF) recorded with a polished aluminum reflector showed a full-width at half-maximum of 40 ps for 315 nm excitation and 50 ps for 360 nm excitation.

Time-resolved exponential decays were fitted by using the global fit procedure of Igor Pro (Wavemetrics). The fitting function was a sum of exponential decays (up to 4 components) convolved with a normalized Gaussian curve of standard deviation σ standing for the temporal IRF and a Heavyside function. All emission decays were fitted using a weighting that corresponds to the standard deviation of the photon number squared root. The lifetimes were shared for all emission wavelengths while the amplitudes were kept as free parameters during the fitting (Levenberg–Marquardt algorithm). Decay Associated Spectra (DAS) were constructed by: $I_i(\lambda) = \alpha_i \tau_i I(\lambda) / \sum \alpha_i(\lambda) \tau_i$, where $I(\lambda)$ is the steady-state emission spectrum and $\alpha_i(\lambda)$ are the wavelength-dependent amplitudes.

Femtosecond Transient Absorption (TA) spectroscopy

The TA set-up is based on a chirped-pulse, regenerative amplifier (Amplitude company) operating at 5 kHz, and producing 800 nm, 40 fs, 0.5 mJ pulses used to pump a Non-collinear Optical Parametric Amplifier (TOPAS; Light Conversion) followed by second harmonic generation.(24) The resulting light beam was tuned at 315 nm or 360 nm and used as pump pulse to excite the samples. As a probe pulse, we have used a chirped, white-light supercontinuum (300–700 nm) produced by focusing a few μJ of the fundamental 800 nm pulse inside a 2 mm thick CaF_2 crystal. The pump and probe are linearly polarized, in magic angle configuration, and focused into a 0.5 mm-thick flow cell where the samples are circulated with a peristaltic pump. The spectrum of the transmitted probe is collected with a spectrograph and a CCD camera. The measured signal corresponds to the pump-induced absorbance ΔA as a function of pump–probe delay τ and probe wavelength λ . The experimental time resolution is 60 to 80 fs. After each TA experiment, we record the solvent signal – sometimes referred to coherent artifact. This signal is used to measure the wavelength dependence of time zero – resulting from the group velocity dispersion of the probe beam(25). We perform conventional TA data analysis, which consists in subtracting this solvent signal from the data recorded on the molecules in solution and post-processing the data to correct the chirp. Then, we perform the global analysis. Singular Value Decomposition (SVD) is used to decompose the data as a product of three matrices: singular spectra, singular values (SV), and singular transients (ST). A global fitting is realized on the two or three dominating ST. The number of STs

considered for the fit is such that the neglected ST's should have an amplitude weaker than the residuals of the global fit. The fitting function is a sum of exponential functions convolved with a Gaussian function modeling the Instrument Response Function (IRF). Up to three time constants are needed to minimize the Chi-square of the global fit. Finally, each time constant determined by the fit, is associated to a Decay Associated Spectrum (DAS) defining the wavelength dependence of the corresponding preexponential factor and therefore the spectral evolution associated to each time constant. For these measurements, ${}^{\text{th}}\text{G}_6$ stock solutions were diluted at a final concentration of 1 mM in aqueous solution (<2% DMSO).

Computational details

Minima characterization. Ground- and excited-state energy minima of the different species were optimized by means of Density Functional Theory (DFT) and its time-dependent version (TD-DFT), using the PBE0(26,27) functional and 6-31+G(d,p) basis set. Their energies (and free energies G^{wa}) were computed by single point calculations using a larger basis set, 6-311+G(2d,2p). To model solvent effects, we resorted to a mixed discrete continuum model, where 6 water molecules were explicitly included in the calculations (Figure 1b) while bulk solvent effects are taken into account by the Polarizable Continuum Model (PCM)(28,29). This computational approach has already profitably been used to study ${}^{\text{th}}\text{G}$, providing an accurate description of the tautomerization equilibria and the electronic spectra(21). We shall use the computed vertical absorption and emission energies to interpret the experimental spectra. Actually, these quantities cannot be directly compared with the absorption and emission maxima, which strongly depend on the vibrational overlap between the different excited states(30). As a consequence, also considering the other possible source of errors of our calculations (density functional, basis set, treatment of solvent effect, lacking of thermal effects), discrepancies of 0.2–0.3 eV between vertical energies and spectral maxima are not surprising and cannot be expected to be the same for all the molecules.

pK_a and lifetimes. For both ground and excited states, pK_a values were obtained using:

$$pK_a = \Delta G^{\text{wa}} / (2.303 RT) \quad (3)$$

ΔG^{wa} corresponds to the free energy difference (in kcal/mol) between the neutral and acidic/basic forms computed in water (using the experimental value, 269 kcal/mol, for the free energy of the H^+ in water)(31,32). We have double-checked our pK_a predictions by using also another procedure(33), which combines ΔG computed in the gas phase at a higher level of theory with differential solvation energies (see SI).

Radiative fluorescence lifetimes were estimated using the protocol described in (21) that considers the emission energies (VEE) and the dipole moments (μ):

$${}^{\text{Theor}}\tau_R = \frac{1}{k_R} \quad k_R = \frac{4 VEE^3}{3 c^3} \mu^2$$

The fluorescence lifetime (τ) can be estimated by considering the experimental quantum yield (Φ) and the relationship below:

$$c\tau = {}^{\text{Theor}}\tau_R \times \Phi$$

Results

Absorption properties

The absorption spectra of ${}^{\text{th}}\text{G}_b$ were recorded in aqueous buffers in the pH range 2–12 (Figure 2A and B). In our previous work,⁽¹⁴⁾ we demonstrated that the spectrum of ${}^{\text{th}}\text{G}$ at pH=7.5 is the sum of two contributions assigned to the H1 and H3 tautomers, characterized by distinct absorption maxima (λ_{max}) at 334 and 313 nm, respectively. The absorption spectra of H1 and H3 were obtained using the excitation spectra at 500 nm and 380 nm, where only H1 and H3 emits, respectively⁽¹⁴⁾. Here we show that for ${}^{\text{th}}\text{G}_b$, the measured spectra and their absorption maxima (Figure 2C) remain almost superimposable within the 6–9 pH range, suggesting that the H1 and H3 tautomers are the only species in this pH range. Their equilibrium is obviously independent of pH in this range, indicating that their interconversion does not involve any protonation or deprotonation step. In addition, the measured spectra for ${}^{\text{th}}\text{G}_b$ tautomers were identical to the one already published⁽¹⁴⁾. In contrast, a progressive blue shift is observed at lower pH values, converging towards a spectrum that is almost superimposable at pH 2 and 3. At the two latter pH values, the position of the absorption maximum (309 nm, Figure 2C) is blue-shifted in respect to the absorption maxima of the H1 and H3 forms (334 and 313 nm, respectively), suggesting that a new species, arbitrarily called the A form, is generated at these acidic pHs. In parallel, a strong red shift accompanied by an absorbance increase is observed at pH > 9, converging towards a spectrum that is almost superimposable at pH 11 and 12. At such basic pHs, the position of the absorption maximum (340 nm, Figure 2C) is significantly red-shifted as compared to the H1 and H3 spectra, indicating that an additional form, called the B form, appears at basic pH. Taken together, our absorption data suggest that in addition to the H1 and H3 tautomers, two additional forms appear at acidic and basic pH. Assuming that the acidic A and basic B forms of ${}^{\text{th}}\text{G}_b$ are the only species in solution at pH 2 and 12, respectively, we could deduce their molar extinction coefficients. Values of $4210 \text{ M}^{-1}\text{cm}^{-1}$ at 309 nm, and $5950 \text{ M}^{-1}\text{cm}^{-1}$ at 340 nm, were obtained for pH 2 and 12, respectively.

Knowing the individual absorption spectra of all four ${}^{\text{th}}\text{G}_b$ species (Figure 3A), we can recover the relative concentrations of the different species in the pH range 2–12 (Figure 3B). The relative concentration of the A form was found to drop at pH>3 and become negligible at pH 6. The B form was observed at pH>9, reaching 100% at pH \geq 11. The relative concentrations of the H3 and H1 tautomers were constant at pH 6–9, being about $43\pm 1\%$ and $57\pm 1\%$,

respectively. Interestingly, the concentrations of both tautomers were found to decrease at pH 4 and 5, as well as at pH 10, but their ratio remained constant. This confirms that the value of the equilibrium constant between the two tautomers, $K=[\text{H1}]/[\text{H3}]=1.33\pm 0.05$, is independent of pH.

Moreover, the changes in the concentrations of both A and B forms with pH can be used to determine their pK_a values using the Henderson–Hasselbalch equation (Fig 3B). The obtained values (4.3 ± 0.1 and 10.2 ± 0.1) are in excellent agreement with those calculated from the pH dependence of the absorption maxima (4.4 ± 0.1 and 10.3 ± 0.1 , Fig. 2C).

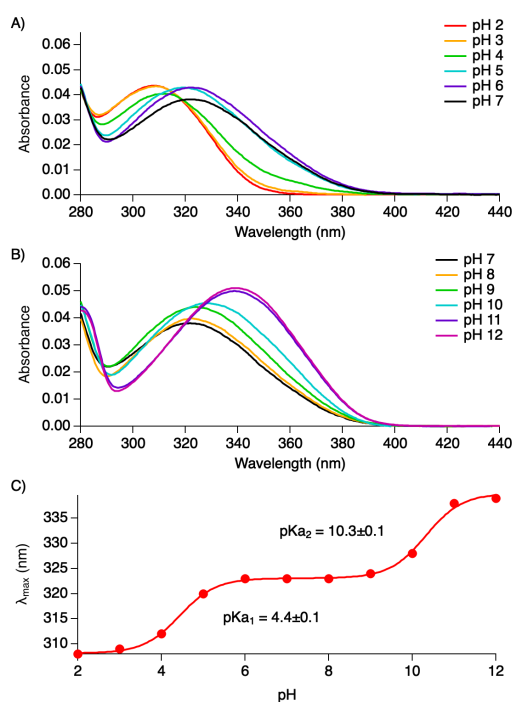


Figure 2: A) and B) Absorption spectra of ${}^{\text{th}}\text{G}_b$ recorded at different pH. C) Dependence of the wavelength of the absorption maximum as a function of pH. The experimental points (red disks) were fitted by the Henderson-Hasselbalch equation (solid line, eq. 1).

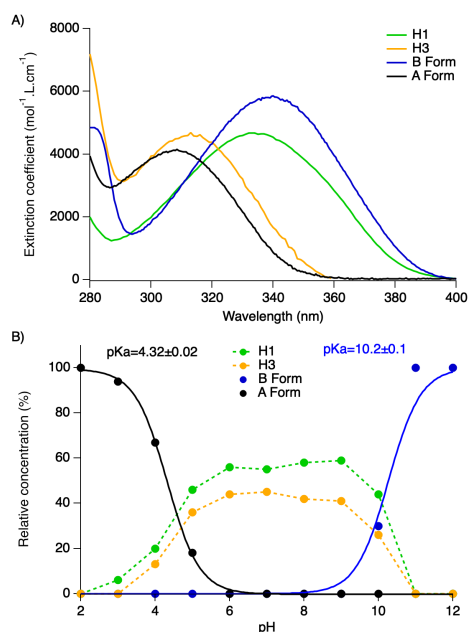


Figure 3: A) Absorption spectra of the four thG_b species. The spectra of the H1 and H3 forms were from Sholokh et al(14), while the spectra of the acidic and basic forms were deduced from the spectra at pH 2 and 12 in Figure 2. B) Concentration profiles of the different thG_b species in the ground state, as obtained from the deconvolution of the spectra in Figure 2A and B. The solid lines correspond to the fit of the experimental points to equation 1.

Emission features

To confirm and further characterize the different forms of thG_b, the emission spectra of thG_b were recorded at different excitation wavelengths selected over the entire absorption spectrum. The emission spectra in the pH range 6–9 (Fig. 4E) were very similar to the previously reported spectra of thG at pH 7.5(14) and exhibited comparable dependence on the excitation wavelength, confirming that the equilibrium between the H1 and H3 tautomers is pH independent in this range.

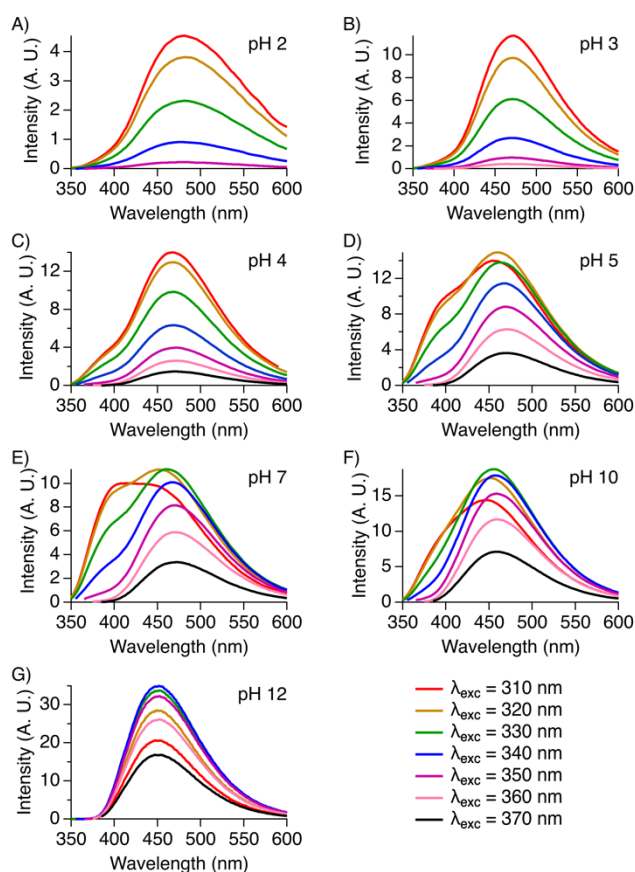


Figure 4: Emission spectra of thG_b recorded at different pH and excitation wavelengths.

At pH 11 and 12, the emission spectra were found to be independent of the excitation wavelength, exhibiting a maximum at 451 nm (Fig 4G) that is clearly distinct from the emission maxima of both the H1 (470 nm) and H3 (400 nm) tautomers. Moreover, the independence of the excitation spectra with respect to the emission wavelength as well as its overlap with the corresponding absorption spectrum (Fig S1A and B) confirm that the B form present in solution at pH=11–12 is a unique species, different from the H1 and H3 tautomers. At pH 10 (Fig. 4F) and excitation wavelengths \geq 350 nm, the emission maximum was at 458 nm, and thus intermediate to that of the H1 tautomer (470 nm) and the B form (451 nm). This strongly suggests that both H1 and B forms are emitting at this pH. Moreover, the H3 emission could be clearly evidenced at pH=10, when the excitation wavelength is below 350 nm. The simultaneous presence of the three forms is further confirmed from the excitation spectra (Fig S2). Indeed, the excitation spectra recorded at 375 nm (Fig S2A) and 450 nm (Fig S2B) overlap well with the absorption spectra of the H3 and B forms, respectively, while the excitation spectrum recorded at 500–550 nm (Fig S2C) is comparable to the absorption spectrum of the H1 tautomer.

Similarly to pH 11 and 12, the emission spectra at pH 2 were independent of the excitation wavelength and showed an emission maximum at 482 nm (Fig 4A). In line with the absorption data, the

emission spectra suggest that the A form contributes to the emission process. In addition, the independence of the excitation spectra on the emission wavelength suggests that only the A form absorbs and emits at pH 2 (Fig S3).

The results obtained at pH 4 and 5 were more difficult to interpret. Though the absorption spectra suggested that the ratio between the H1 and H3 concentrations was constant over the pH range 4–10, we clearly observed that the relative contribution of the emission of the H3 tautomer decreased at pH 4 and 5 (compare Fig 4C and D with Fig. 4E). Moreover, at pH 3, although the contribution of the H1 tautomer was less than 10% in the absorption spectrum, the emission spectra were found to be independent on the excitation wavelength and to fully overlap with the emission spectrum of the H1 tautomer (Fig 4B). The clear discrepancy between the absorption and emission data at pH 3–5 thus suggests a possible excited-state reaction, which accumulates the H1 tautomer.

We then characterized the fluorescence quantum yields of ${}^{\text{th}}\text{G}_b$ as a function of pH. For each pH value, we determined the QYs at multiple excitation wavelengths (310–340 nm at pH 2 and 3, and 310–370 nm at pH 4–12). At all pH values, the QY values were found to be constant over the explored excitation wavelength range. Moreover, the QY values were found to be remarkably constant (0.48 ± 0.03) over the pH range 5–12 (Fig S4). As in the pH range 6–9, only the H1 tautomer is excited at wavelengths ≥ 350 nm, while both H1 and H3 tautomers are excited at lower wavelengths, this clearly indicates that both H1 and H3 tautomers possess the same QY (0.48 ± 0.03). This conclusion is in line with our previous contribution, where a QY of $0.49 (\pm 0.03)$ was reported for both H1 and H3 tautomers of ${}^{\text{th}}\text{G}$ at pH 7.5(14). Moreover, as only the B form is observed at pH 12, while the B form is mixed with the H1 and H3 tautomers at pH 10 and 11, the constancy of the QY value at pH 10–12 strongly suggests that the QY of the B form is identical to that of the H1 and H3 tautomers. In contrast, the A form exhibits a substantially lower QY (0.11 ± 0.01), as measured at pH 2. Knowing the percentages of H1, H3 and A forms in the ground state at pH 3–5 (Fig 3B) and the QYs of the three forms, it is easy to calculate the QYs that would be expected in this pH range if no excited state reaction would occur. The calculated values (0.13, 0.23 and 0.41 at pH 3, 4 and 5, respectively) are markedly lower than the experimental ones (0.3, 0.42, and 0.48), suggesting that the A form must be converted in one of the other forms in the excited state.

Time-resolved spectroscopy

To gather additional information on the excited-state reaction at acidic pH and the photophysics of ${}^{\text{th}}\text{G}_b$, its time-resolved fluorescence decays were analyzed. First, we recorded spectrally resolved fluorescence decays as a function of pH (4–12) upon excitation at 360 nm. As depicted in Figure 3A, only the H1 tautomer and the B form absorb at this wavelength. For each pH value, $I(\lambda, t)$ was fitted using a global analysis algorithm. The lifetimes were kept constant

for all pH and λ values and the amplitudes were the only free parameters of the fit. The DAS were calculated as described in the materials and methods section. Within the pH range 4–9, the fluorescence decays were characterized by a single fluorescence lifetime of 20.5 ns attributed to H1*, the excited-state of the H1 tautomer (Fig. 5A–B). A similar behavior was also observed at $\text{pH} \geq 11$, where the fluorescence decays displayed a single component (13.5 ns) that can be associated to the decay of B*, the excited-state of the B form (Fig. 5D). At pH 10, the decay was nicely fitted by a bi-exponential function (13.5 and 20.5 ns were fixed), suggesting that both H1* and B* forms emit (Fig 5C).

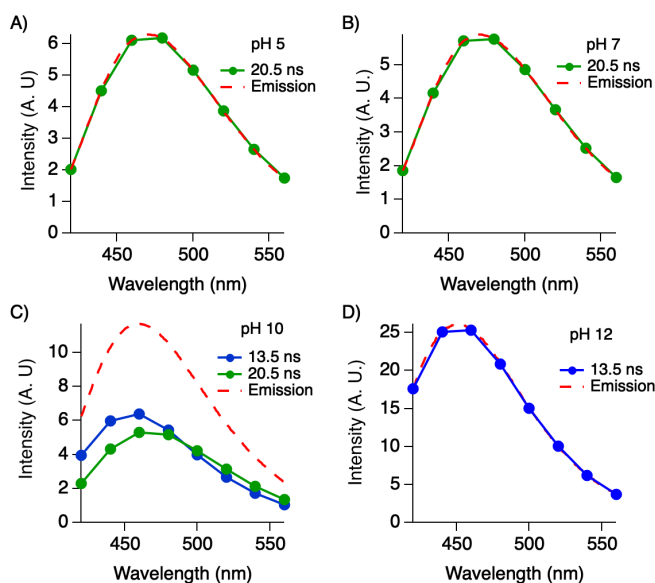


Figure 5: A-D) Decay associated spectra obtained at pH 5, 7, 10 and 12, upon excitation at 360 nm. The spectrally resolved fluorescence decays were analyzed by using the global fit algorithm as described in the main text.

Next, we performed spectrally resolved fluorescence decay measurements as a function of pH (2–12) upon 315 nm excitation, where all the species absorb (Fig 3A).

Within the pH range 6–9, the fluorescence decays were fitted to a two-component model with decay times of 20.5 ns (fixed as obtained from the experiments performed upon excitation at 360 nm) and 12.6 ns (Fig. 6A, B and C). As the DAS of the shorter component corresponded well to the emission spectrum of the H3, this shorter component could be unambiguously attributed to this tautomer. To exclude the possibility of an ultra-fast conversion between the two tautomers in their excited state (i.e. faster than the 40 ps temporal resolution of our TCSPC set-up), TA spectroscopy measurements (80 fs resolution) were performed at pH 7 ($\lambda_{\text{exc}}=315$ nm). The results are shown in Fig. 7A. The TA signal is dominated by a strong excited-state absorption band over the whole spectral range (325–600 nm) which does not show any spectral change, but a monotonous slow decrease with time that is consistent with the long-lived lifetimes of the H1

and H3 forms. This clearly shows the absence of excited-state conversion between H1 and H3.

At pH 10, the emission and excitation spectra indicate that emission from H1, H3 and B are observed at this pH value. As the lifetime of the H3* (12.6 ns) and B* (13.5 ns) are too close to be resolved, we fixed them (together with the lifetime of H1* i.e. 20.5 ns) in the analysis of the fluorescence decays. From the global analysis of the decays recorded across the emission spectrum of thG_b, we obtained three DAS that match very well with the emission spectra of the three forms (Fig 6D). As for the 360 nm excitation, the fluorescence decay at pH≥11 displayed a single component (13.5 ns) that can be attributed to the emission of B* (Fig. 6E).

At pH 2, the measured fluorescence decays were analyzed using the global fit method by sharing the lifetimes (floating parameters) between all wavelengths. Three components were required to accurately fit the measured decays. The two short-lived lifetimes (0.14 and 1.1 ns) exhibited a positive amplitude in the blue part of the spectrum and a negative one in the red part of the spectrum. This suggests the existence of at least one excited-state reaction, where A (that absorbs with a maximum at 309 nm, Fig. 3A) is likely converted into other species, which yield an emission spectrum centered at 481 nm (Fig. 4A). The long-lived component (7 ns) was found to be largely dominant and is likely associated to the species produced through the excited state reaction. To further support this excited-state conversion, TA spectroscopy measurements were performed. In contrast to the data at pH=7, the TA spectrum measured at pH=2 (Fig. 7B, 7C, 7D) shows a clear conversion between two different spectroscopic signatures with a 50-ps timescale (see Fig 7D). This conversion is followed by a slow decay, consistent with the 7 ns component measured by TCSPC. A depletion in the early ESA signal is observed around 400 nm (green band at delays < 10ps in Fig. 7B) and is likely associated to the stimulated emission from A*, overlapping the ESA signal in this spectral range.

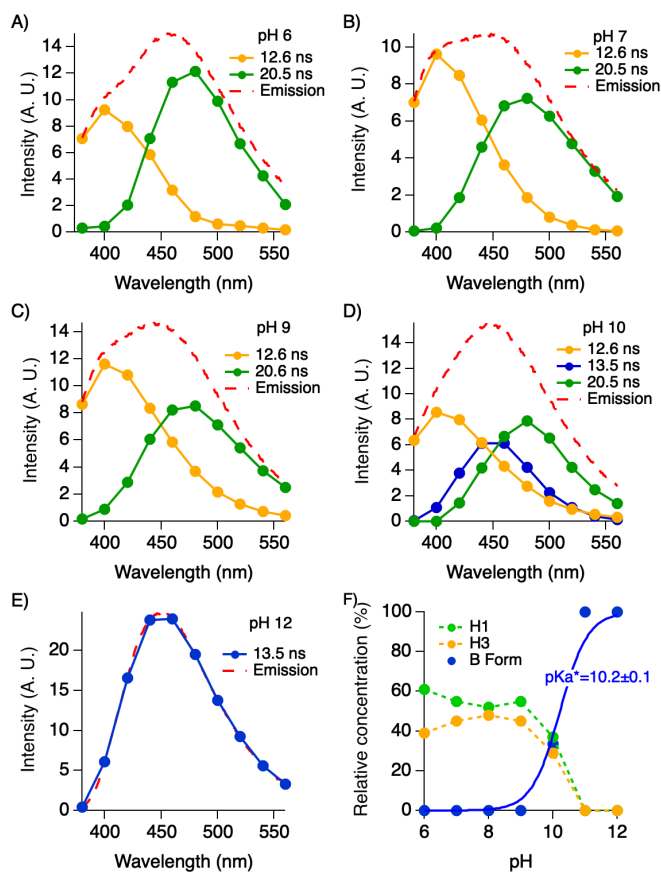


Figure 6: A–E) Decay associated spectra determined at pH 6, 7, 9, 10 and 12, upon excitation at 315 nm. The spectrally resolved fluorescence decays were analyzed by using the global fit algorithm as described in the main text. F) Relative concentrations of the different thG_b species in the excited state obtained from the DAS corrected from the differences in the extinction coefficients.

Three components are required to accurately fit the fluorescence decays obtained at pH 3, namely the two short-lived lifetimes (0.14 and 1.1 ns) associated to the excited-state reaction and a long-lived lifetime (14.8 ns). At pH 4, H3 is already present in the ground state (12.6 ns) and is therefore significantly contributing to the fluorescence decays. Hence, the fit of the data provided 4 components (0.14, 1.1, 12.6 and 19.7 ns). At pH 5, the decays were largely dominated by the contributions of H3 (12.6 ns) and H1 (20.5 ns) associated to their direct excitation, so that it was no more possible to detect any short-lived lifetime. Our time-resolved measurements support thus a model in which an excited state reaction is taking place at low pH. As a result, as already reported for other compounds(24,34), the measured fluorescence lifetimes should depend on the lifetimes of the interconverting species and the excited-state kinetic constants that rule their interconversion. This hypothesis would be consistent with the increase of the longest lifetime from 7 ns (pH 2) to 20.5 ns (pH 5).

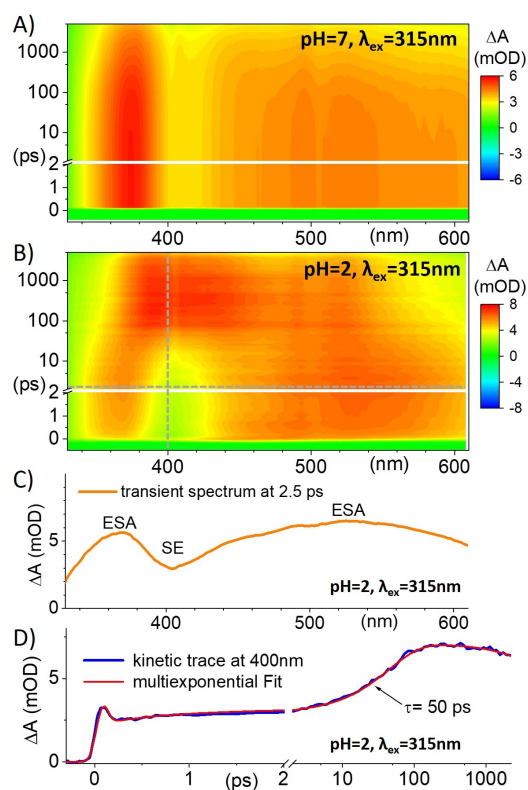


Figure 7: TA spectroscopy of ${}^{\text{th}}\text{G}_b$ upon excitation at $\lambda_{\text{ex}}=315\text{nm}$: 2D maps of the TA signal (ΔA , color scale) as a function of probe wavelength (nm) and pump-probe delay (ps) measured at A) pH=7 and B) pH=2. The signal is everywhere positive (red), i.e. dominated by strong excited-state absorptions (ESA). The horizontal and vertical dashed lines in panel B respectively illustrate the time delay of 2.5 ps at which we plot the transient spectrum in panel C, and the wavelength of 400 nm at which we monitor the decay kinetics in panel D. We identify the green region seen in panel B around 400 nm at early time delays to be the stimulated emission (SE, negative signal) of species A^* , which is overlapping its positive and more intense ESA at the same wavelength. The result of the global fitting (see “Experimental section”) is illustrated in panel D (red line). Following fast spectral relaxation within the first 1 ps (likely due to intramolecular and/or solvent relaxation), a time constant of (48 ± 2) ps is determined and assigned to the excited state conversion kinetics of A^* .

Calculations

Ground state species and absorption properties

Supporting the results obtained for the ${}^{\text{th}}\text{G}$ nucleoside(21), only the H1 and H3 tautomers of ${}^{\text{th}}\text{G}_b$ are populated at neutral pH, the former being slightly more stable, in agreement with the experimental observations (Table S1 in SI). The computed vertical absorption energies are in good agreement with the experimental absorption spectra, but with a small overestimation (0.3 eV) of the transition energy of H3 (Table 1).

As a first step to the study of ${}^{\text{th}}\text{G}_b$ in basic pH, we have considered the possible species corresponding to the anionic form of ${}^{\text{th}}\text{G}_b$ (Fig. S5). As shown in Table S1, the most stable species is predicted to be the keto-amino one, where both N1 and N3 are deprotonated. This form, labelled as $[{}^{\text{th}}\text{G}_b]^-$, should be the only one populated in basic conditions and thus correspond to the B form. This attribution is strengthened by the good match of the computed vertical absorption energy for this species with the experimental absorption maximum at high pH (Table 1).

For acidic solutions, we have characterized the three possible forms for a protonated ${}^{\text{th}}\text{G}_b$ (Figure 1a). The most stable (Table S1) is the one where both N3 and N1 atoms are protonated, hereafter labeled as $[{}^{\text{th}}\text{G}_b\text{-H1-H3}]^+$. It is at least 0.4 eV more stable than the other two possible forms, suggesting that it should be the only one at low pH and thus correspond to the A form. Moreover, the absorption maximum computed for $[{}^{\text{th}}\text{G}_b\text{-H1-H3}]^+$ provides an intense transition at 306 nm, in excellent agreement with the experimental absorption maximum at low pH (Table 1). The absorption maxima computed for the two other forms were in lesser agreement with the experiments, supporting our assignment.

		Theoretical				Experimental			
FC	S_1 min	ΔE (Stokes Shift)	f	τ_r	Absorption	Emission	Stokes Shift	τ_r	
H1									
3.76 (329)	2.99 (414)	0.77	0.0668	16 (a)	3.73 (334)	2.65 (470)	1.08	20	
H3									
4.23 (293)	3.40 (364)	0.83	0.0855	9 (a)	3.96 (313)	3.10 (400)	0.86	13	
$[{}^{\text{th}}\text{G}_b\text{-H1-H3}]^+$									
4.05 (306)	3.24 (382)	0.81	0.0534	- (c)	4.00 (309)				
$[{}^{\text{th}}\text{G}_b\text{-H1-OH}]^+$									
3.24 (382)	2.58 (479)	0.66	0.0460	8 (b)		2.57 (482)		7	
$[{}^{\text{th}}\text{G}_b\text{-H3-OH}]^+$									
3.81 (325)	3.00 (412)	0.81	0.0546	5 (b)					
$[{}^{\text{th}}\text{G}_b]^-$									
3.78 (328)	3.06 (405)	0.72	0.0949	10 (a)	3.64 (340)	2.74 (451)	0.90	13	

Table 1. Computed absorption (Franck Condon geometry) and emission (S_1 min) energies in eV (nm), Stoke shift, oscillator strength (f) and radiative lifetimes of different forms of ${}^{\text{th}}\text{G}_b$ at the TD-PBE0/6-311+G(2d,2p)//PBE0/6-31+G(d,p) level of theory, explicitly including 6 H_2O molecules and PCM into the calculations. Fluorescence lifetimes were calculated assuming quantum yield of (a) 0.5 or (b) 0.1. (c) presumably very low fluorescence QY due to excited state reaction, as evidenced by TA and time-resolved fluorescence experiments.

Interestingly, the computed pKa's (3.2 for H1 and 4.2 for H3) are fully consistent with the experimental ones, considering the presence of two almost equipopulated tautomers at neutral pH and the intrinsic

difficulty in accurately computing pK_a values in solution (see SI for a detailed discussion).

Excited state species and emission properties

Geometry optimizations of the lowest energy bright excited state of H1 and H3 (identified as H1* and H3*) lead to stable minima of the Potential Energy Surface (PES), in line with the substantial experimental quantum yield of both tautomers. The computed emission energies and Stokes shift match fairly well with their experimental counterpart (Table 1)(21).

For the emission of ${}^{\text{th}}\text{G}_b$ at basic pH, geometry optimization of $[\text{thG}_b]^-$ leads to a stable minimum of the PES, characterized by a strong emission at 3.06 eV ($f=0.095$). We have also optimized the minima of the bright excited state of four other possible forms. Based on their relative stabilities (Table S1), emission energies (Table S2) and associated lifetimes, we can conclude that only the S_1 minimum of $[\text{thG}_b]^-$ contributes to the fluorescence of ${}^{\text{th}}\text{G}_b$ at high pH.

We have next optimized the minima of the spectroscopic state for the three possible species at acidic pH. The computed emission energy for $[\text{thG}_b\text{-H1-H3}]^{*+}$ (the most stable in the ground state) is 382 nm. This value matches well with the negative signal appearing at ~ 400 nm in the early TA spectrum (Figure 7B and 7C), which could be then assigned to stimulated emission from this species. On the other hand, it does not match the steady state emission spectrum, being significantly blue-shifted (Figure 4A). Our calculations predict, in fact, that the bright excited state minimum of the $[\text{thG}_b\text{-H1-OH}]^{*+}$ form is more stable by 0.3 eV (Table S1) compared to $[\text{thG}_b\text{-H1-H3}]^{*+}$, suggesting that $[\text{thG}_b\text{-H1-OH}]^{*+}$ plays a major role in the emission of ${}^{\text{th}}\text{G}_b$ at acidic pH. This conclusion is further substantiated by the computed emission wavelength (479 nm) from the minimum of $[\text{thG}_b\text{-H1-OH}]^{*+}$ that almost coincides with the experimental maximum (482 nm) (Table 1). In contrast, the minimum of $[\text{thG}_b\text{-H3-OH}]^{*+}$ is the least stable and should not be involved in the photophysics of ${}^{\text{th}}\text{G}_b$.

Finally, by computing the radiative lifetime of the different excited states and using the measured QYs, we predicted the fluorescence lifetimes of the different species (Table 1). Comparison with the experimental lifetimes shows reasonable agreement, correctly predicting that H1 has a longer lifetime than H3. Our calculations are also in good agreement with experiments for the B form; the estimated fluorescence lifetime being close to the experimental value.

Discussion

In this study we explored the photophysical properties of ${}^{\text{th}}\text{G}_b$, a highly emissive G analog, as a function of pH. At neutral pH, the absorption and emission properties of ${}^{\text{th}}\text{G}_b$ were found to be very similar to those previously reported for the ${}^{\text{th}}\text{G}$ ribonucleoside(13)

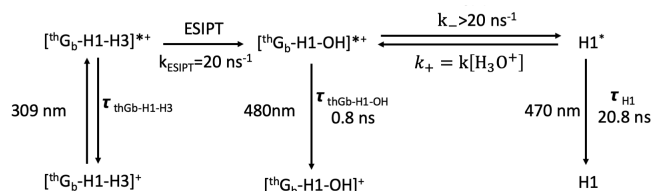
and deoxyribonucleoside(14,17,35). This indicates that as for other fluorescent nucleobases(8,36), the sugar does not substantially alter the photophysical properties of the aromatic chromophore.

The DAS and deconvoluted emission spectra were used to determine the relative contributions of the different species in the excited state (Fig. 6F). The percentages were corrected using the differences in the extinction coefficients between the different forms (Fig.3A). At the 6–9 pH range, the percentages of the two tautomers as deduced from the DAS and the deconvoluted emission spectra match well with those obtained from the absorption data, confirming that we have two tautomers in equilibrium in the ground state, with $K=[\text{H1}]/[\text{H3}]=1.3\pm 0.1$, and indicating that no interconversion occurs in the excited state. The ground-state equilibrium between H1 and H3 is also fully supported by the *ab initio* calculations. As each of the two tautomers is excited and emits independently from the other one, the kinetic rate constants governing the equilibrium between the two forms are likely slow with respect to the excited state lifetime. Indeed, no interconversion is observed in the excited state, as shown by the TA data (Fig. 7A) and by the fact that excitation of only the H1 tautomer at wavelengths ≥ 350 nm does not generate any emission from the H3 tautomer. A good match is seen for the population of the B, H1 and H3 forms at pH 10, as obtained from the absorption spectra, the deconvoluted emission spectra and the DAS. Moreover, the ratio between the H1 and H3 tautomers is about 1.2 and matches well with the equilibrium constant between the two forms. The data at pH 10 strongly suggest that the equilibrium between the H1 and H3 tautomers and the B form attributed to the $[\text{thG}_b]^-$ anion is a ground-state equilibrium. The pK_a^* value (10.2 ± 0.1) calculated from the DAS (Fig. 6F) is in perfect agreement with the pK_a value calculated from the absorption data (10.2 ± 0.1) and computed from the Förster cycle theory or quantum mechanical calculations (Table S4), confirming that the conversion occurs in the ground state. As a result, each of these forms is excited and emits independently, from the two others. Finally, in line with the pK_a values, both the absorption and emission spectra indicate that the H1 and H3 tautomers are fully converted into the $[\text{thG}_b]^-$ anion at $\text{pH} \geq 11$.

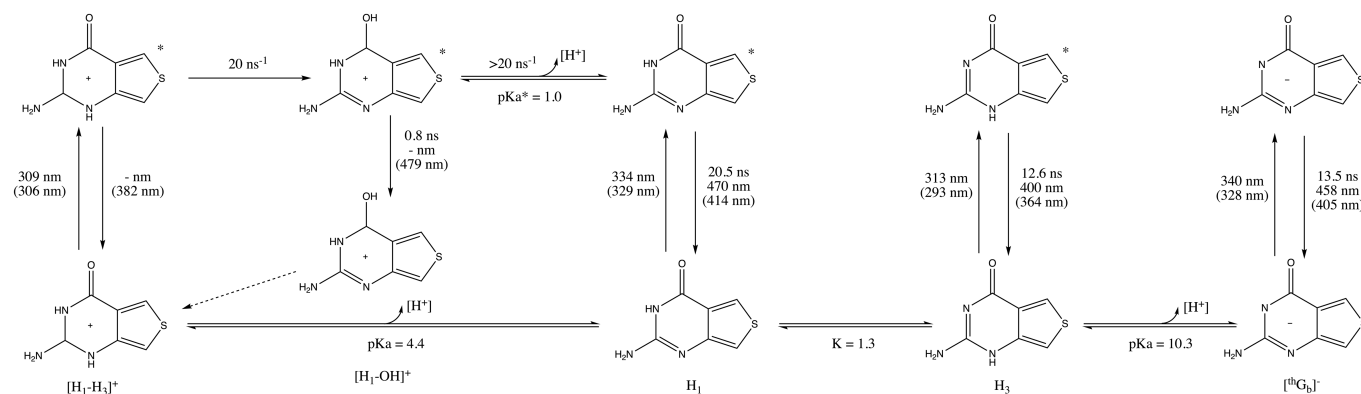
At acidic pHs, two short-lived lifetimes that displayed positive and negative amplitudes over the studied spectral range were identified, suggesting an excited-state reaction. From quantum mechanical calculations, this reaction was assigned to the conversion of $[\text{thG}_b\text{-H1-H3}]^{*+}$, the excited-state of the $[\text{thG}_b\text{-H1-H3}]^+$ into the excited-state of $[\text{thG}_b\text{-H1-OH}]^+$. The computed absorption maximum of $[\text{thG}_b\text{-H1-H3}]^+$ and emission maxima of both $[\text{thG}_b\text{-H1-H3}]^{*+}$ and $[\text{thG}_b\text{-H1-OH}]^{*+}$ were consistent with the experimental data. Moreover, $[\text{thG}_b\text{-H1-OH}]^+$ was found to further convert in the excited state into the H1 tautomer as evidenced by the increase of the long-lived lifetime that reach 20.5 ns at pH 5. Finally, at pH 4 and 5 it was possible to fit the fluorescence decays by including and fixing the lifetime of H3 (12.6 ns), likely indicating that H3 absorbs and emits independently from the other two forms and is therefore not involved in the proton

transfer process. Interestingly, the quantum mechanical calculations predict a clear decrease of the pK_a^* (2.8) as compared to the pK_a in the ground state (4.4 ± 0.1).

Based on these data, we developed the global model shown in Scheme 1 to describe the photophysics of ${}^{\text{th}}\text{G}_b$ in acidic pHs (<6). In this model, the excited state $[{}^{\text{th}}\text{Gb-H1-H3}]^{**}$ can convert into the more stable form $[{}^{\text{th}}\text{Gb-H1-OH}]^{**}$ through an excited-state intramolecular proton transfer (ESIPT). As evidenced by TA experiment performed at pH 2, the ESIPT rate was fixed to 20 ns^{-1} in our model. At the same time, as the excited-state pK_a^* value is lower than the ground-state pK_a value, $[{}^{\text{th}}\text{Gb-H1-OH}]^{**}$ can undergo a water-mediated excited-state proton transfer (ESPT) to produce H1^* . In the proposed model, the water-mediated back-proton transfer (associated to the H1^* conversion into $[{}^{\text{th}}\text{Gb-H1-OH}]^{**}$) is pH dependent and thus governed by an apparent constant ($k_+ = k[\text{H}_3\text{O}^+]$), where $[\text{H}_3\text{O}^+]$ is the concentration of protons in buffer.



Scheme 1: Photocycle model used to describe the emission properties of ${}^{\text{th}}\text{G}_b$ in acidic conditions. The equilibria in the ground-state are not indicated.



Scheme 2: Proposed photophysics of ${}^{\text{th}}\text{G}_b$ in aqueous solution

The kinetic rate constants and fluorescence lifetimes obtained through this approach are gathered in Table S6 and Scheme 1. Interestingly, the calculated lifetime value of H1 is very close to the

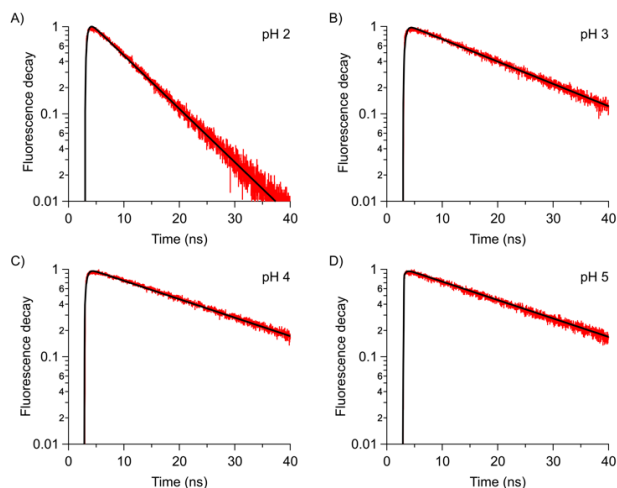


Figure 8: A–D) Fluorescence decays recorded at pH 2, 3, 4 and 5 (red curves). Excitation and emission wavelengths were at 315 nm and 480 nm, respectively. The solid black lines correspond to the fits using the numerical integration of the differential equation system described in the SI and the values given in Table S6 and scheme 1.

To validate this model, the fluorescence decays in the pH range 2–5 were fitted by numerically solving the set of coupled differential equations given in the SI. The decays used for the fits were recorded with an excitation at 315 nm and an emission at 480 nm, to account for the decays of both $[{}^{\text{th}}\text{Gb-H1-OH}]^{**}$ and H1^* forms. Using our model, it was possible to obtain the time-dependent concentrations of the different species in the excited-state after the initial pulsed excitation (40 ps). By considering that the fluorescence decays measured at 480 nm are proportional to the excited state populations ($[{}^{\text{th}}\text{Gb-H1-OH}]^{**}$ and H1^*) generated by exciting $[{}^{\text{th}}\text{Gb-H1-H3}]^+$ plus the fraction of H1 directly excited at 315 nm (relative contribution displayed in Fig. 3B), we were able to fit the fluorescence decays (Figure 8) and determine the kinetic rate constants.

experimental one. Moreover, the ratio k_+/k_- was found to change by 10-fold for each pH change by one unit, in full line with the change in proton concentration as predicted by our model. Finally, the model

validity was further substantiated by calculating a pK_a^* value of 1.0 from the ratio of the ESPT rate constants, in reasonable agreement with the calculated pK_a^* (2.8). Finally, both ESPT and ESPT reactions occur on sub-50 ps timescale in perfect agreement with values found in literature for organic compounds(24)(37).

Conclusions

We have used a combination of spectroscopic techniques and quantum mechanical calculations to investigate the photophysical properties of the ${}^{\text{th}}\text{G}_b$ nucleobase at various pHs. This allowed us to identify three new species for ${}^{\text{th}}\text{G}_b$ and characterize their photophysics in both the ground- and excited-states (scheme 2). We found that at pH 6–9 the absorption and emission properties were dominated by the previously identified H1 and H3 tautomers, which are in equilibrium in the ground-state and do not interconvert during their fluorescence lifetime. At basic pH, these ground-state tautomers deprotonate into $[\text{thG}_b]^-$ ($pK_a = 10.2$). Similarly to neutral pH, no excited-state reaction appears to occur between the different tautomers at basic pH. At acidic pH, the ground-state H1 and H3 tautomers are converted into the protonated and blue-shifted $[\text{thG}_b\text{-H1-H3}]^+$ species ($pK_a = 4.3$). A more complex picture appears in the excited state at these acidic pHs, as $[\text{thG}_b\text{-H1-H3}]^{*+}$ appears to tautomerize to $[\text{thG}_b\text{-H1-OH}]^{*+}$ through an ESPT reaction and is then converted into H1* through a water-mediated ESPT reaction. As the identified species differ by their spectra and their fluorescence lifetime, ${}^{\text{th}}\text{G}_b$ may be used as a local probe for sensing pH changes. The probe would be especially useful in the 2–6 pH range, where dramatic photophysical changes can be perceived.

Conflicts of interest

There are no conflicts to declare.

Acknowledgements

We thank Dr Thomas Gustavsson for discussion and preliminary time-resolved femtosecond experiments. This work was supported by the Agence Nationale de la Recherche (ANR blanc PICO2 and SMFLUONA), the Labex NIE and the Centre National pour la Recherche Scientifique (CNRS). Y. M. is grateful to the Institut Universitaire de France (IUF) for support and providing additional time to be dedicated to research. YT thanks the National Institutes of Health for support (via grant number GM 069773).

Notes and references

- McKinney SA, Déclais A-C, Lilley DMJ, Ha T. Structural dynamics of individual Holliday junctions. *Nat Struct Biol.* févr 2003;10(2):93-7.
- Kaushik M, Kaushik S, Roy K, Singh A, Mahendru S, Kumar M, et al. A bouquet of DNA structures: Emerging diversity. *Biochem Biophys Res. mars* 2016;5:388-95.
- Aznauryan M, Sønndergaard S, Noer SL, Schiøtt B, Birkedal V. A direct view of the complex multi-pathway folding of telomeric G-quadruplexes. *Nucleic Acids Res.* 15 déc 2016;44(22):11024-32.
- Dzatko S, Krafcikova M, Hänsel-Hertsch R, Fessl T, Fiala R, Loja T, et al. Evaluation of the Stability of DNA i-Motifs in the Nuclei of Living Mammalian Cells. *Angew Chem Int Ed.* 19 févr 2018;57(8):2165-9.
- Lilley DMJ. Structures of helical junctions in nucleic acids. *Q Rev Biophys.* mai 2000;33(2):109-59.
- Sholokh M, Sharma R, Grytsyk N, Zaghzi L, Postupalenko VY, Dziuba D, et al. Environmentally Sensitive Fluorescent Nucleoside Analogues for Surveying Dynamic Interconversions of Nucleic Acid Structures. *Chem - Eur J.* 18 sept 2018;24(52):13850-61.
- Wilhelmsson LM. Fluorescent nucleic acid base analogues. *Q Rev Biophys.* mai 2010;43(2):159-83.
- Jones AC, Neely RK. 2-aminopurine as a fluorescent probe of DNA conformation and the DNA–enzyme interface. *Q Rev Biophys.* mai 2015;48(2):244-79.
- Sinkeldam RW, Greco NJ, Tor Y. Fluorescent Analogs of Biomolecular Building Blocks: Design, Properties, and Applications. *Chem Rev.* 12 mai 2010;110(5):2579-619.
- Dallmann A, Dehmel L, Peters T, Mügge C, Griesinger C, Tuma J, et al. 2-Aminopurine Incorporation Perturbs the Dynamics and Structure of DNA. *Angew Chem Int Ed.* 9 août 2010;49(34):5989-92.
- Xu W, Chan KM, Kool ET. Fluorescent nucleobases as tools for studying DNA and RNA. *Nat Chem.* nov 2017;9(11):1043-55.
- Wilhelmsson M, Tor Y. Fluorescent analogs of biomolecular building blocks: design and applications [Internet]. Hoboken, NJ: Wiley; 2016 [cité 23 sept 2019]. Disponible sur: <http://public.eblib.com/choice/publicfullrecord.aspx?p=4453524>
- Shin D, Sinkeldam RW, Tor Y. Emissive RNA Alphabet. *J Am Chem Soc.* 28 sept 2011;133(38):14912-5.
- Sholokh M, Improtta R, Mori M, Sharma R, Kenfack C, Shin D, et al. Tautomers of a Fluorescent G Surrogate and Their Distinct Photophysics Provide Additional Information Channels. *Angew Chem Int Ed.* 4 juill 2016;55(28):7974-8.
- Han JH, Park S, Hashiya F, Sugiyama H. Approach to the Investigation of Nucleosome Structure by Using the Highly Emissive Nucleobase ${}^{\text{th}}\text{dG}$ –tC FRET Pair. *Chem – Eur J.* 16 nov 2018;24(64):17091-5.

16. Kilin V, Gavvala K, Barthes NPF, Michel BY, Shin D, Boudier C, et al. Dynamics of Methylated Cytosine Flipping by UHRF1. *J Am Chem Soc.* 15 févr 2017;139(6):2520-8.
17. Park S, Otomo H, Zheng L, Sugiyama H. Highly emissive deoxyguanosine analogue capable of direct visualization of B–Z transition. *Chem Commun.* 2014;50(13):1573.
18. Li Y, Fin A, McCoy L, Tor Y. Polymerase-Mediated Site-Specific Incorporation of a Synthetic Fluorescent Isomorphous G Surrogate into RNA. *Angew Chem Int Ed.* 24 janv 2017;56(5):1303-7.
19. Shin D, Lönn P, Dowdy SF, Tor Y. Cellular activity of siRNA oligonucleotides containing synthetic isomorphous nucleoside surrogates. *Chem Commun.* 2015;51(9):1662-5.
20. Han JH, Yamamoto S, Park S, Sugiyama H. Development of a Vivid FRET System Based on a Highly Emissive dG-dC Analogue Pair. *Chem - Eur J.* 1 juin 2017;23(31):7607-13.
21. Martinez-Fernandez L, Gavvala K, Sharma R, Didier P, Richert L, Segarra Martí J, et al. Excited-State Dynamics of Thienoguanosine, an Isomorphous Highly Fluorescent Analogue of Guanosine. *Chem – Eur J.* 28 mai 2019;25(30):7375-86.
22. Melhuish WH. QUANTUM EFFICIENCIES OF FLUORESCENCE OF ORGANIC SUBSTANCES: EFFECT OF SOLVENT AND CONCENTRATION OF THE FLUORESCENT SOLUTE ¹. *J Phys Chem.* févr 1961;65(2):229-35.
23. Lakowicz JR. Principles of fluorescence spectroscopy. 3rd ed. New York: Springer; 2006. 954 p.
24. Skilitsi AI, Agathangelou D, Shulov I, Conyard J, Haacke S, Mély Y, et al. Ultrafast photophysics of the environment-sensitive 4'-methoxy-3-hydroxyflavone fluorescent dye. *Phys Chem Chem Phys.* 2018;20(11):7885-95.
25. Kovalenko SA, Dobryakov AL, Ruthmann J, Ernsting NP. Femtosecond spectroscopy of condensed phases with chirped supercontinuum probing. *Phys Rev A.* 1 mars 1999;59(3):2369-84.
26. Perdew JP, Burke K, Ernzerhof M. Generalized Gradient Approximation Made Simple [Phys. Rev. Lett. 77, 3865 (1996)]. *Phys Rev Lett.* 17 févr 1997;78(7):1396-1396.
27. Adamo C, Scuseria GE, Barone V. Accurate excitation energies from time-dependent density functional theory: Assessing the PBE0 model. *J Chem Phys.* 15 août 1999;111(7):2889-99.
28. Miertuš S, Scrocco E, Tomasi J. Electrostatic interaction of a solute with a continuum. A direct utilization of AB initio molecular potentials for the prevision of solvent effects. *Chem Phys.* févr 1981;55(1):117-29.
29. Tomasi J, Mennucci B, Cammi R. Quantum Mechanical Continuum Solvation Models. *Chem Rev.* août 2005;105(8):2999-3094.
30. Avila Ferrer FJ, Cerezo J, Stendardo E, Improta R, Santoro F. Insights for an Accurate Comparison of Computational Data to Experimental Absorption and Emission Spectra: Beyond the Vertical Transition Approximation. *J Chem Theory Comput.* 9 avr 2013;9(4):2072-82.
31. Topol IA, Tawa GJ, Burt SK, Rashin AA. On the structure and thermodynamics of solvated monoatomic ions using a hybrid solvation model. *J Chem Phys.* 22 déc 1999;111(24):10998-1014.
32. Tissandier MD, Cowen KA, Feng WY, Gundlach E, Cohen MH, Earhart AD, et al. The Proton's Absolute Aqueous Enthalpy and Gibbs Free Energy of Solvation from Cluster-Ion Solvation Data. *J Phys Chem A.* oct 1998;102(40):7787-94.
33. Saracino GAA, Improta R, Barone V. Absolute pKa determination for carboxylic acids using density functional theory and the polarizable continuum model. *Chem Phys Lett.* mai 2003;373(3-4):411-5.
34. Chou P-T, Pu S-C, Cheng Y-M, Yu W-S, Yu Y-C, Hung F-T, et al. Femtosecond Dynamics on Excited-State Proton/ Charge-Transfer Reaction in 4'-N,N-Diethylamino-3-hydroxyflavone. The Role of Dipolar Vectors in Constructing a Rational Mechanism. *J Phys Chem A.* mai 2005;109(17):3777-87.
35. Sholokh M, Sharma R, Shin D, Das R, Zaporozhets OA, Tor Y, et al. Conquering 2-Aminopurine's Deficiencies: Highly Emissive Isomorphous Guanosine Surrogate Faithfully Monitors Guanosine Conformation and Dynamics in DNA. *J Am Chem Soc.* 11 mars 2015;137(9):3185-8.
36. Reichardt C, Wen C, Vogt RA, Crespo-Hernández CE. Role of intersystem crossing in the fluorescence quenching of 2-aminopurine 2'-deoxyriboside in solution. *Photochem Photobiol Sci.* 2013;12(8):1341.
37. Kumpulainen T, Rosspeintner A, Dereka B, Vauthey E. Influence of Solvent Relaxation on Ultrafast Excited-State Proton Transfer to Solvent. *J Phys Chem Lett.* 21 sept 2017;8(18):4516-21.